5 Potentiometric Microsensors for *In Situ* Measurements in Aquatic Environments

D. DE BEER
Max Planck Institute for Marine Microbiology, Bremen, Germany

1 INTRODUCTION

The objective of this chapter is to relate a short overview of potentiometric principles to measurements with ion-selective microsensors. Potentiometric analyses are based upon measurement of the potential difference of an electrochemical cell in the absence of current. With this method, ion concentrations are measured using ion-selective membrane electrodes. These electrodes provide a rapid and convenient way for measuring a range of anions and cations (see Table 1 for examples). Miniaturization of some of these sensors to microelectrodes is a recent development. Although the principles are the same,

In Situ Monitoring of Aquatic Systems: Chemical Analysis and Speciation Edited by J. Buffle and G. Horvai.

Table 1. Overview of compounds measurable with potentiometry. Selectivity coefficients are determined with the separate solution method. The values in bold are estimated from the maximum ratio ($c_{\text{interferent}}/c_{\text{analyte}}$) for which interference is negligible [1]. The underlined compounds must be absent for reliable determination of the analyte.

Analyte	Detection limit (mol L^{-1})	Interfering compounds ($\log(K_{i,j}$ / L mol^{-1}))	References
Br^-	5×10^{-6}	CN^-**(4)**, I^- **(4)**, Cl^-**(−2)**, OH^-**(−4)**, $\underline{S^{2-}}$	1
BF_4^-	10^{-5}	$ClO_4^-(3)$, $I^-(2)$, $ClO_3^-(1)$, $CN^-(0)$, $Br^-(-1)$, $NO_2^-(-1)$, $NO_3^-(-2)$, $HCO_3^-(-2)$, $Cl^-(-2)$, $SO_4^{2-}(-4)$	1
Ca^{2+}	10^{-8}	$H^+(-2.5)$, $Na^+(-5.8)$, $K^+(-7.2)$, $Mg^{2+}(-6.7)$, $Ba^{2+}(-2.5)$, $NH_4^+(-3.6)$, $Mn^{2+}(-1.6)$, $Co^{2+}(-4.6)$	2
Cd^{2+}	10^{-7}	$\underline{Hg^{2+}, Ag^+, Cu^{2+}}$	1, 3–5
Cl^-	5×10^{-5}	$\underline{CN^-(-7)}$, $\underline{I^-(-7)}$, $Br^-(-3)$, $S_2O_3^{2-}(-2)$, OH^-**(2)**, $\underline{S^{2-}}$	1
CN^-	10^{-6}	I^-**(1)**, Br^-**(−3)**, *Cl^-***(6)**, $\underline{S^{2-}}$	1
Cu^{2+}	10^{-8}	$\underline{Hg^{2+}, Ag^+, Cu^+}$	1, 4, 5
CO_2	10^{-6}	H_2S (0.3)	6, 7
F^-	10^{-6}	$OH^-(-3)$	1
H^+	10^{-12}	$Na^+(-13, -14)$	8
K^+	10^{-6}	$H^+(-3.4)$, $Na^+(-4.1)$, $Mg^{2+}(-5.7)$, $Ca^{2+}(-5.2)$	9
Mg^{2+}	10^{-6}	$H^+(1.7)$, $Na^+(-3.8)$, $Li^+(-3.1)$, $Ca^{2+}(0)$	10
Na^+	3×10^{-5}	$H^+(0.5)$, $Li^+(-1.6)$, $K^+(-0.4)$, $NH_4^+(-0.9)$, $Mg^{2+}(-3.6)$, $Ca^{2+}(-3.3)$	11
NH_4^+	10^{-6}	$H^+(-1.8)$, $Li^+(-2.4)$, $Na^+(-2.7)$, $K^+(-0.9)$, $Mg^{2+}(-5.5)$, $Ca^{2+}(-3.8)$	12
NO_2^-	10^{-8}	$SCN^-(0.3)$, $I^-(-2)$, $HCO_3^-(-2.2)$, $ClO_4^-(-2.5)$, $Br^-(-3)$, $NO_3^-(-3.2)$, $Cl^-(-3.2)$, $SO_4^-(-3.5)$, $\underline{S_2O_3^{2-}}$, $\underline{S^{2-}}$	13
NO_3^-	10^{-5}	$\underline{I^-(1)}$, $\underline{NO_2^-(-1)}$, $Cl^-(-2)$, $HCO_3^-(-3)$, acetate(−3)	14
HPO_4^{2-}	10^{-6}	$Cl^-(-2.3)$, $NO_3^-(-2.8)$, $SO_4^{2-}(-3)$, lactate(−3), $SCN^-(-2.3)$, acetate(−3.2)	15
S^{2-}	10^{-6} (total sulfide, pH 7)	$\underline{Hg^{2+}}$, $\underline{O_2}$	16, 17

preparation and use of potentiometric microsensors requires special equipment, training and patience of the researcher.

As potentiometric microsensors are much more fragile, noise sensitive and difficult to prepare than macrosensors, they are not the instruments of choice for routine water analysis. For that purpose it is better to use either macrosensors or alternative analytical techniques. Microsensors should be used when spatial resolution is needed, i.e. for measurements of steep gradients at interfaces. As steep gradients are usually caused by microbial processes, potentiometric microsensors for aquatic environments are still typical research tools, almost exclusively used for microbiological studies.

2 POTENTIOMETRIC SENSORS

The potentiometric sensors relevant for environmental monitoring are generally ion-selective membrane electrodes. The following discussion will be limited, therefore, to this class of potentiometric sensors.

2.1 PRINCIPLES OF POTENTIOMETRY

Potentiometric determinations are based on the measurement of an electrical potential difference across a selective membrane. An example of a measuring circuit is:

ref 1 | 3 mol L^{-1} KCl | filling electrolyte | ion-selective membrane | sample | **3 mol L^{-1} KCl | ref 2**

where the underlined part is the ion-selective sensor and the bold part the external reference electrode. In Figure 1 the measuring circuit for potentiometric sensors is sketched. Ref 1 and ref 2 indicate connections between the electrolytes and the wiring, usually an Ag/AgCl or calomel electrode. Ref 1 is the internal reference element located inside the measuring electrode; ref 2 is part of the external reference electrode.

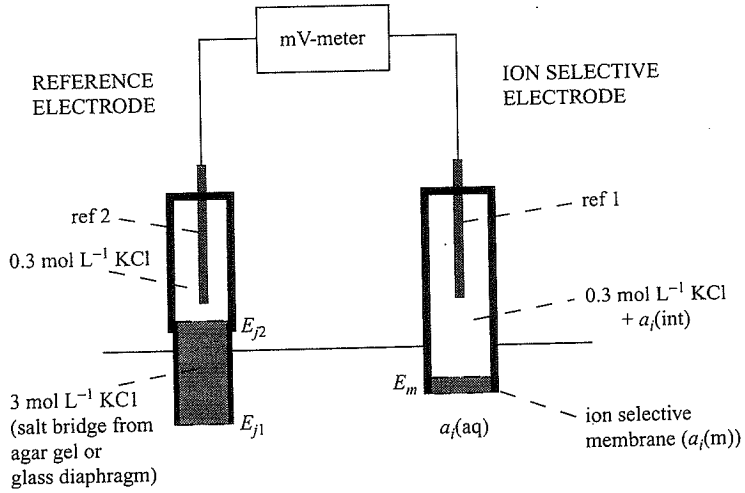

Figure 1. Measuring circuit for potentiometric sensors. E_m = membrane potential, E_{j1}, E_{j2} = liquid junction potentials, a_i(aq), a_i(m), a_i(int) = activitiy of ion i in the test aqueous solution, in the membrane, and in the internal solution, respectively

The reference electrodes, which have a constant potential relative to the solution they contact, can be either calomel or Ag/AgCl half-cells. The Ag/AgCl is most widely used as it equilibrates faster than calomel electrodes after a temperature change [8] and is easy to integrate in sensors. The external reference electrode is connected to the sample by a salt bridge, a glass diaphragm or an agar gel with 3 mol L^{-1} KCl.

The electrical potential drop across this circuit is the sum of all individual contributions, of which most are sample independent and thus constant. The measured potential is then

$$\Delta E = E_{\text{const}} + E_{\text{j1}} + E_{\text{m}} \tag{1}$$

where E_{j1} is the junction potential between sample and reference, and E_{m} is the membrane potential. E_{j1} is small and is almost constant if 3 mol L^{-1} KCl is used in the salt bridge, therefore, E_{m} determines the response of the circuit. While previously E_{m} was described as the sum of the two interface potentials and the diffusion potential inside the membrane, it is now recognized that the inner phase boundary potential can be considered as constant and the diffusion potential in the membrane as negligible. Thus, in most cases, the phase boundary potential at the sample side of the membrane is the main determinant of E_{m} and thus of the sensor response, ΔE [18]. In ref. [18], the authors derived from thermodynamic considerations an expression for the phase boundary potential, E_{PB}:

$$E_{\text{PB}} = -\frac{\mu_i^{\text{p}}(\text{org}) - \mu_i^{\text{p}}(\text{aq})}{zF} + \frac{RT}{zF}\ln\frac{a_i(\text{aq})}{a_i(\text{m})} \tag{2}$$

where μ is the chemical potential, a_i the activity of the ion i in the sample (aq) and membrane (m), R is the gas constant, T the absolute temperature, z the algebraic charge number of the ion, F the Faraday constant. Under the further condition that $a_i(\text{m})$ remains constant, the Nernst equation is obtained

$$\Delta E = E^\circ + \frac{RT}{zF}\ln a_i(\text{aq}) \quad \text{or} \quad \Delta E = E^\circ + k \log a_i(\text{aq}) \tag{3}$$

where E° is the offset potential, i.e. the potential difference across the cell when $a_i = 1$, and k is the slope factor equal to 59.16 z^{-1} mV at 25 °C.

The essential condition for the phase boundary potential model, that the membrane composition remains constant, is met by a series of conditions. The membrane must have ion-exchange or complexing properties, and the main determinant for $a_i(\text{m})$ is the concentration of the corresponding sites in the membrane. The membrane must also be hydrophobic, to prevent co-extraction of the counter-ions. If these conditions are not met, $a_i(\text{m})$ will be proportional to $a_i(\text{aq})$. Incorporation of an ionophore that selectively binds the analyte ion

ensures that $a_i(\text{m})$ remains constant in the presence of interfering ions. The ionophore thus determines the selectivity of the sensor.

The phase boundary model as described above explains and predicts the behavior of ion-selective membrane sensors better than the ion-translocation model [19]. For example, the short response time of liquid membrane sensors is incompatible with the transport of ions through thick membranes, and the need for lipophilic ions of opposite charge as membrane components.

In practice, ideal Nernst behavior (equation (3)) is not always observed. Particularly, deviations from the Nernst equation become significant at low activities. The deviations are explained by additional contributions to ΔE, in particular liquid junction potentials, E_{j1} and E_{j2}, phase boundary potentials due to interfering ions, and potential leaks (Figures 1 and 2) [19]. E_{j1} is dependent on the sample composition, but this dependence can be made almost negligible by using a high concentration salt bridge, such as 3 mol L^{-1} KCl which is normally used. The junction potential between the salt bridge and the sample is dominated by the diffusivity of K^+ and Cl^-, and since these are approximately equal, E_{j1} becomes close to zero. E_{j2} is constant since the composition of the salt bridge and the internal solution of the reference electrodes are constant. The contributions to ΔE by interfering ions are expressed by the Nicolskii–Eisenman equation:

$$\Delta E = E^{\circ\prime} + k \log\left(a_i + \sum K_{i,j}(a_j)^{z_i/z_j}\right) \tag{4}$$

with $E^{\circ\prime}$ the observed offset potential, K_{ij} the selectivity factor of ion i over j and a_j the activities of interfering ions. As pointed out by Bakker *et al.* (1997) the Nicolskii–Eisenman formalism is inconsistent when $z_i \neq z_j$. They solved this problem using the phase boundary potential model, for which the reader is referred to the relevant literature [18].

The reference electrode is usually a commercial Ag/AgCl or a calomel half-cell. It is a mistake to position the external reference very close to the measuring electrode. First of all, the level of the internal electrolyte of the reference electrode should be above the sample solution to avoid contamination of the electrolyte by analyte solution and dilution of the salt bridge. In the case of *in situ* measurements at large depth the reference should be slightly pressurized to avoid this effect, especially in freshwater environments [8]. Secondly, for measurements in sediments, biofilms or microbial mats, the reference electrode should not be pushed into the matrix. Then the 'suspension effect' can change the junction potential between the salt bridge and the sample, especially when colloids are present [8]. This poorly understood phenomenon can result in a considerable change in offset. The suspension effect changes only the potential of the reference electrode, i.e. the junction potential at the salt bridge, but not the potential of the ion-selective electrode.

2.2 OVERVIEW OF EXISTING MICROSENSORS

In many aquatic systems conversions mainly take place in the sediments, microbial mats and biofilms covering the sediments and solid surfaces, instead of in the water phase. Because of mass transfer limitations inside these structures, gradients of substrates and products are present, the concentrations of substrates being lower and the concentrations of products higher than in the water phase. The slope of the concentration gradients depends on the conversion rates and mass transfer rates. Significant changes can occur within 10 μm in highly active biofilms while in less active deep-sea sediments significant changes occur typically within millimeters to centimeters. In such systems porewater analysis has limitations. The extraction of porewater may influence the concentration profiles and in the case of biofilms its spatial resolution is insufficient. Thus *in situ* measurements are needed with high spatial resolution, of at least 50 μm. The best technique available nowadays is the use of microsensors, needle-shaped devices with a tip size of 1–20 μm which can measure the concentration of a specific compound. Owing to the small sensing tip, highly localized measurements are possible, since the spatial resolution should be approximately equal to the tip size of the sensor. There are indications, however, from theoretical and experimental studies that microsensors can influence the concentration profiles. The evidence is conflicting: while the theory predicts underestimation especially by sensors larger than 10 μm [20], experiments with O_2 microsensors in a biofilm showed an overestimation of local concentrations by sensors larger than 16 μm [21]. Microsensors may change the local concentrations by the consumption of substrate (in the case of amperometric sensors), by compression of the local matrix [22], by changing the diffusion field (blocking diffusion by the sensor body) [20], or by compressing the boundary layer [23]. Although the microelectrode technique is invasive and the tips have a small influence on structures and processes, it is the best choice for direct concentration measurements inside biofilms, mats and sediments.

Microsensors were introduced in microbial ecology by Bungay *et al.* (1969) [24] who measured O_2 profiles in biofilms. The technique was strongly improved by Revsbech who constructed reliable O_2 microsensors for profiling sediments and biofilms [25,26]. More microsensors relevant for microbial ecology were developed and used, such as for N_2O [27], pH [28], NH_4^+ [29], NO_3^- [30–32], S^{2-} [33], H_2S [34], NO_2^- [35], CH_4 [36], Ca^{2+} [2] and CO_2 [6].

A survey of the compounds which can be measured with membrane electrodes (see Table 1 and list of microsensors for microbial ecology above) showed that they can be grouped in three, rather distinct, clusters corresponding to the three groups of elements in the periodic system: (I) elements from the alkali and alkaline earth metal groups, (II) b-metals, (III) elements in the top right corner of the periodic system (with the exclusion of the noble gases, but including the halogens, C, N, O and S). Important elements such as iron, manganese and

silicon are placed far from these clusters in the periodic system, which makes the prospects of measuring these elements with potentiometric methods rather poor. Iron and manganese can be measured by stripping voltammetry [37], but the technology has not yet been applied to needle-type microsensors.

There are several different types of potentiometric microsensors. Their miniaturization is described below.

(1) Crystalline membrane. These membranes consist, e.g. of metal halides and respond to the concentration of the halogen and metal ion in the sample. Lists of sensor types based on this principle can be found in reviews [38]. Only the Ag_2S membrane sensor has been miniaturized. The sensor responds to Ag^+ and S^{2-}. This microelectrode has been useful in studies of the sulfur cycle in microbial mats and biofilms. The application and peculiarities of this sensor are discussed in Chapter 4.

(2) Full glass. Glass membrane sensors are described for Na^+, K^+ and H^+ [39] and all have been miniaturized, mainly for use in animal physiology [39]. As Na^+ or K^+ microgradients do not normally occur in sediments, mats and biofilms, only the pH microsensor is useful for environmental application. The full glass pH microsensor can be used for many purposes [40], but because of its rather large (50–100 μm long) sensing tip, it has a rather low spatial resolution. The long tip responds to the pH gradient along the length of the sensing surface, but it averages in an unknown way. Thus it is impossible to resolve pH differences within a distance of less than the tip length. Using the recessed tip principle, for which the sensor tip is placed in a casing with a small opening at the tip, can considerably increase the spatial resolution [39]. However, this increases the response time considerably. The pH sensor is discussed in detail in Chapter 3.

(3) Liquid membranes. These can be divided into classical ion-exchanging membranes and carrier-based membranes. The ion-exchanging membranes contain hydrophobic ions (ion-exchanger ions) and the analyte counter-ion. Carrier-based membranes contain complexes between specifically binding hydrophobic agents (also called ionophores) and the analyte ion. The ion specific behavior of liquid membranes with dissolved carrier was discovered in 1967 [41], and later these membranes were incorporated in micro-pipettes [42]. In the past, liquid membrane macrosensors for water analysis have been sold commercially. The liquid membrane microsensor technique was developed by cell physiologists for intracellular measurements (mostly H^+, CO_3^{2-}, Mg^{2+}, Ca^{2+}, Li^+, Na^+ and K^+) [39, 43, 44]. These sensors can be very small, with a tip diameter of less than 1 μm, i.e. the size of a bacterial cell. Relevant liquid membrane microsensors for use in microbial ecology are NH_4^+ [29], NO_3^- [30], NO_2^- [35, 45], H^+ [46], Ca^{2+} [2], and CO_3^- [47]. The CO_2 microsensor [6] is a special electrode, with a liquid membrane pH sensor as transducer. As H^+ and CO_2 microsensors are treated in Chapter 2, this chapter will focus on liquid membrane sensors for determination of N-compounds and Ca^{2+}.

2.3 LIQUID MEMBRANE MICROSENSORS

Potentiometric microsensors function in the same way as macrosensors, although they deviate more often from ideal behavior, because of their small tip size. Liquid membrane microelectrodes consist of a glass micropipette with ion-exchanging liquid in the tip acting as the functional membrane. The potential build up by the membrane may be dissipated through the glass wall of the micropipette and through the shunt between the ion-exchanging membrane and the glass wall (see Figure 2) [48]. Obviously, miniaturization increases the occurrence of leaks as the ratio of the tip surface to the total capillary surface decreases. Consequently, for some microsensors a relatively large tip is required. For example, NO_2^- sensors are only functional if the tip is at least 10 μm [35]; smaller sensors only respond to concentrations above 100 μmol L^{-1} [45]. However, Ca^{2+} microsensors with 1 μm tips function excellently, having fast response ($t_{90} < 1$ s) at low concentrations (< 1 μmol L^{-1}) [2]. The selectivity is partially an intrinsic property of the membrane and partially determined by the size and shape of the sensor. Generally, the smaller the size of a sensor, the worse the selectivities, as non-specific ion exchange in the glass wall and between the liquid membrane and the glass wall more strongly contributes to the signal. Also, the quality of the silanization may vary, as it is a poorly controllable process, influenced (in a way that is not fully understood) by local temperature, humidity, and shape of the tip [48]. In the author's experience, the best results (with respect to the ease of filling with membrane,

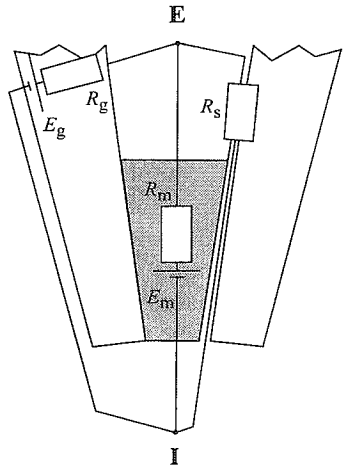

Figure 2. The electrical components of a potentiometric microsensor. E_m = membrane potential, R_m = membrane resistance, E_g = glass potential (potential by ion exchange through glass), R_g = resistance of glass wall, R_s = resistance shunt (seal between membrane and glass wall). I denotes sample, E sensor electrolyte

Table 2. Selectivity coefficients of liquid membrane microsensors (approximate values)

Cation sensors	$\log(K_{i,Na^+})$	$\log(K_{i,K^+})$	$\log(K_{i,H^+})$	$\log(K_{i,Ca^{2+}})$	$\log(K_{i,L_i^+})$	$\log(K_{i,Mg^{2+}})$	References
H^+	−10	−10	–	−11	−10	?	46, 49, 50
Ca^{2+}	−6	−5	−4	–	?	−7	2, 51
NH_4^+	−2	−1	−4	−5	−4	−6	29, 52
Anion sensors	$\log(K_{i,Cl^-})$	$\log(K_{i,HCO_3^-})$	$\log(K_{i,HS^-})$	$\log(K_{i,NO_2^-})$	$\log(K_{i,NO_3^-})$	$\log(K_{i,SO_4^{2-}})$	
NO_3^-	−2	−3	?	−2	–	−3	14, 30, 53
NO_2^-	−5	−4	poisoned	–	−5	−6	13, 35

signal stability, detection limit, sensor lifetime and physical strength of tip) are obtained if the tip is tapered between 5 and 10°. In Table 2 a list of selectivity coefficients for microsensors is given. The values are approximate, and may vary slightly between individual microsensors. In actual practice, with Ca^{2+} and N– compound microelectrodes, determination of the selectivity factors for each microsensor is not needed. A calibration performed in a solution with the same composition as the sample (but with adjusted concentrations of the analyte) is sufficient, thereby determining $E^{o\prime}$, k and the concentration range within which the electrode can be used. Ca^{2+} sensors used in seawater can be calibrated in water with the main salts present in seawater. pH microsensors used in seawater should be calibrated in special seawater buffers. NH_4^+, NO_3^- and NO_2^- sensors used for waste water biofilm research can be calibrated in artificial waste water containing the main constituents of the actual waste water in which the measurements are performed. This way of calibrating is reliable, if the interfering ions are constant in background, i.e. if there are no gradients of interfering species. Then their contribution to the signal ($\sum K_{i,j}(a_j)^{z_i/z_j}$ in equation (4)) is constant at each point in the profile. The strongest interfering species for NH_4^+ are Na^+ and K^+, which are not consumed or produced in microbial processes, and therefore constant over the distance over which the profiles are measured (typically a few mm). The strongest interfering species for NO_3^- are ClO_4^-, SCN^-, I^- and Cl^- that are normally not present in significant quantities in the freshwater environments where nitrate sensors are used. Except in biofilms converting halogenated substrates Cl^- is not usually a biological product, so no gradients can be expected. HCO_3^- has been reported as interfering with the measurements of NO_3^-, and being a major product of microbial conversion it can lead to errors. The error is strongly dependent on the selectivity of the ion-exchanging membrane, as will be discussed later.

Although the electrodes respond to the activity of the ion, electrodes are usually calibrated for concentration as under life-sustaining (low ionic strength, pressure and temperature) conditions activity coefficients are approximately constant. The calibration is log–linear over a concentration range depending on

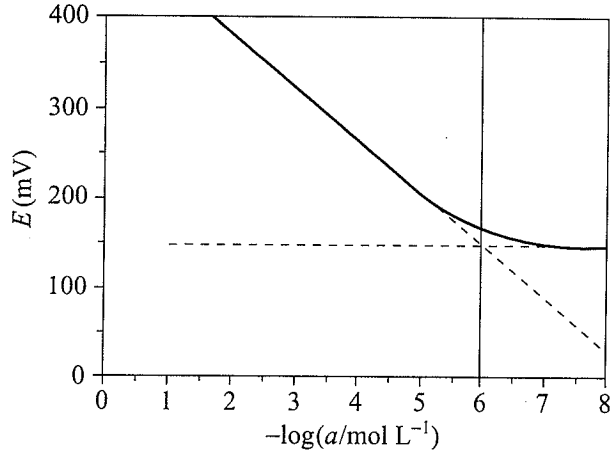

Figure 3. Typical response curve of a potentiometric sensor. The detection limit is given by the intercept of the dashed lines

the composition of the medium. At lower concentrations the calibration tapers off and finally the sensor becomes insensitive to concentration change (Figure 3). The intercept of the linear parts of the log–linear response curve is the detection limit. However, the curved part of the calibration line can be used below this concentration thereby extending the actual measuring range 1 decade below the detection limit (albeit with reduced accuracy). In medium where the analyte is complexed however, the use of the curved part of the calibration plot is not recommended.

It should be kept in mind that potentiometric sensors respond to the activity of the free ions. This is important for Ca^{2+} which easily binds to various organic molecules. Consequently, Ca^{2+} profiles measured with microsensors may not represent the total mobile concentration. This should be considered for correct estimation of the fluxes. This may especially occur in organic-rich sediments and biofilms in reactors with high organic loading. Also NH_4^+ can bind to sediments, particularly to clay and humic substances.

2.3.1 Membrane Chemistry

Cations. For cations, carrier-based liquid membrane sensors are used, in which the selectivity of the membrane is determined by a lipophilic ligand that complexes reversibly and specifically with the measured ion. The carrier–ion complex is so strong that the concentration of free ions in the membrane is negligible compared with the concentration of ions bound in the complex. This is an important difference with the classical ion-exchanging membranes (see

below). Most relevant carrier-based liquid membrane sensors for microbial ecology measure H^+, NH_4^+ and Ca^{2+}. The response time (t_{90}) is expressed as the time needed to reach 90% of the signal change after a step change in concentration. According to the phase boundary model, transport in the sensor should not play a role. Since the membrane phase boundary has a thickness of a few nm, transport through the aqueous diffusion layer surrounding the microsensor should limit the response time [18]. Then sensors with a tip size of 1–3 μm should have a t_{90} of the order of 1–100 ms. However, usually the response time is of the order of seconds, so what actually affects the response time of ion-selective sensors is not well understood. The response time is influenced by the tip size of the sensor (which determines the electrical resistance of the measuring system) and the capacitance of the measuring circuit. However, this effect occurs if the tip size is 1 μm or less, while for environmental studies, sensors have tip sizes of 3 μm, and relatively low tip resistance. The response time of the nitrite sensor depends on the concentration and varies from 15 s in the μmol L^{-1} range to 1 s in the mmol L^{-1} range; for other microsensors it is of the order of 1 s over the whole concentration range.

Anions. For anions, usually classical ion-exchanging membranes are used based on lipophilic salts (e.g. quaternary ammonium salt) that act as exchanger sites. In these membranes complexation between the anions and cationic sites in the membrane phase is negligible, so that all anions are freely dissolved in the membrane. They all exhibit the same selectivity sequence with a preference for lipophilic over hydrophilic ions, following the Hofmeister series:

$$ClO_4^- > SCN^- > I^- > NO_3^- > NO_2^- > Cl^- > HCO_3^- > SO_4^{2-} > HPO_4^{2-}$$

The selectivity is determined by the distribution coefficient of the anions between sample solution and membrane, which is mainly determined by the standard Gibbs energy for transfer of the ion from the water phase into the membrane (for full treatment of this issue see Koryta (1983), pp. 30–39) [54]. Although the membrane composition has an effect on the selectivity coefficients, the selectivity sequence cannot be changed. This is demonstrated in Figure 4, which shows the selectivity of various membrane chemistries for a variety of ions. As a consequence of this fixed sequence of selectivities, the only sensor based on this principle, useful for environmental application, is the NO_3^- sensor, often applied in freshwater sediments and biofilms. The strongest interference can be expected from ClO_4^-, SCN^- and I^- species which are not common in freshwater environments. Also carbonate sensors and their use in animal physiology, have been described [47]. Because of their sensitivity to NO_3^- they cannot be used in aquatic environments. Innovations for anion sensors (deviations from the Hofmeister series) can only be expected from development of anion-selective carriers. The use of tri-*n*-octyltin chloride

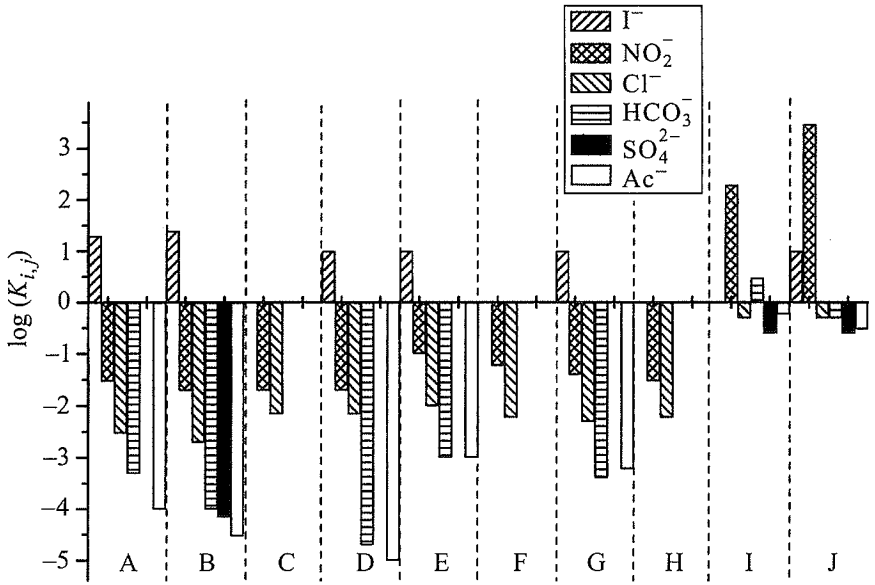

Figure 4. Selectivity coefficients of various liquid ion exchange membranes (LIX), measured in microelectrodes (except for G and J) with the separate solution method. (A) 10% Co(III)-iodo-salocden in nitrophenyl octyl ether (NPOE) [55], (B) as for (A) but 20% [55], (C) 20% Co(III)-triphenylphosphine-bromo-salocden in NPOE [55], (D) 20% Co(III)-methoxo-salocden in NPOE [55], (E) Orion exchanger [55], (F) Orion exchanger [30], (G) Crytur [55], (H) Radiometer [53], (I) 9% aquocyanocobalt(III)-hepta(2-phenylethyl)cobyrinate in NPOE [45], (J) 1% aquocyanocobalt(III)-hepta(2-phenylethyl)cobyrinate in NPOE [45]. (I) and (J) are carrier-based membranes.

increased the selectivity towards HCO_3^- ions [9], although no application of this carrier has been reported. A lipophilic vitamin B12 derivative proved to be a highly selective carrier for NO_2^- (Figures 4 and 5) [13]. The developments of phosphate ionophores [15, 56] and a promising sulfate carrier [44] have been reported; however, sensor applications based on these compounds have not yet been published.

Carrier-based liquid membranes consist of an inert, viscous, non-volatile and hydrophobic solvent, such as 2,3–dimethylnitrobenzene, *o*-nitrophenyl *n*-octyl ether (most widely used), bis(1–butylpentyl)adipate or bis(2-ethylhexyl)sebacate in which the lipophilic complexing agents are dissolved. Addition of lipophilic anions (such as sodium tetraphenylborate or potassium tetrakis(*p*-chlorophenyl)borate) has been shown to be essential for the carrier-based sensor characteristics by increasing the selectivity and reducing the response times [19]. As is now understood, the lipophilic ions act as ion-exchangers needed for the functioning of the membrane [18]. Finally, addition of poly(vinyl

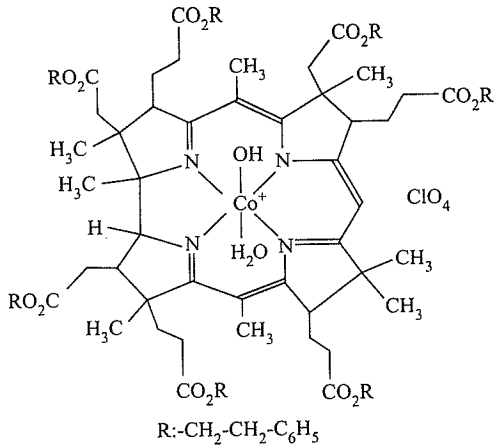

Figure 5. Nitrite ionophore used in liquid membranes. It is a vitamin B12 derivative to which alkyl groups are attached to make the complex hydrophobic. The nitrite ion is thought to complex by exchange with an axial ligand of the Co^{3+} [13]

chloride) (PVC) improves the signal stability, lifetime and sensitivity of the sensor. Solidification of the liquid membrane physically stabilizes the membrane in the tip. Furthermore, the tip of the microcapillary gets coated by liquid membrane which decreases the ion-exchange through the thin glass wall. The PVC is dissolved in tetrahydrofuran (THF) and mixed with the liquid membrane. This cocktail is brought into the tip of the microsensor and after evaporation of the THF a solid membrane remains. Without addition of PVC the tip size cannot be larger than 1 μm, as in larger tips the capillary force is too weak to maintain the membrane. Solidification allows preparation of larger sensors (3–20 μm), that are stronger than 'real' microsensors with 1 μm tips.

2.3.2 Preparation of Liquid Membrane Microsensors

The preparation of liquid membrane microsensors involves pulling of the capillaries, silanization of the glass, shielding, filling with electrolyte and liquid membrane, and application of a coating. The liquid membrane microsensors were originally developed for intracellular measurements. These sensors were of simple design, consisting of a silanized capillary with a tip size of less than 1 μm, filled with electrolyte and with a droplet of ion-exchanger in the tip. Such sensors are extremely fragile and noise sensitive. Thus experiments have to be performed in a Faraday cage for noise protection, and measurements must be done in a quiet working environment. Moreover, these sensors will break often in sediments. For experiments in environmental samples the sensor

manufacturing has been modified to make them more sturdy and less noise sensitive. The following procedure can be used for all types of liquid membrane sensors, that differ only in the filling electrolyte and membrane.

Glass tubing (e.g. 3.5 mm OD, 8516 Schott) is heated in a flame and pulled to a thickness of ca. 1 mm over a length of ca 20 cm. The capillary is further pulled in an electrical heating loop to a thickness of ca. 200 μm. Then, using a thin platinum heating loop mounted on a micromanipulator, the glass is elongated until a thickness of ca. 30 μm is reached. Then the heat of the loop is reduced, the loop is moved slowly closer to the glass until it falls off. The capillary should gradually taper to a 1–3 μm tip.

To stabilize the hydrophobic membrane in the tip of the microcapillary the glass must be made hydrophobic by a silanization procedure. The capillaries are baked in a glass container (2–3 L) at 150 °C for 3 h, to remove bound water. Then 250 μL *N,N*-dimethyltrimethylsilylamine (Fluka) is added and the closed container is left overnight at 200 °C. An alternative procedure is dipping the freshly pulled microcapillaries in trichlorosilane, followed by baking at 125 °C for 15 min. This procedure is faster, but with inferior results [48]. The silanized capillaries are glued with silicone glue in a glass shielding made from Pasteur pipettes, with the tips protruding 1–2 cm [53]. The finished pipettes can be stored dry and dust-free for an unlimited time.

Before filling, the tips can be broken to the desired size. For most sensors 1–3 μm tips are ideal, for NO_2^- sensors the tip should be 10–15 μm. Breaking is done under microscopic guidance, by moving gently against a clean Pasteur pipette. The sensor tips are filled with the appropriate electrolyte over a length of ca. 4 cm. The electrolyte contains usually 5–50 mmol L^{-1} of the ion measured, or for pH sensors a pH buffer with 300 mmol L^{-1} KCl. Then some liquid membrane without PVC is introduced in the tip (ca. 300 μm). Additionally, 100–200 μm of the PVC-containing liquid membrane is introduced. After ca. 2 h the THF is evaporated and a solidified ion-selective membrane is left in the tip. In the author's experience, liquid membranes completely gelled with PVC are not stable in capillaries larger than 1 μm. The membrane often loosens from the glass wall, or is upon immersion partially extruded through the tip, for unknown reasons. Only the combination of PVC gelled and non-gelled liquid membrane results in functional sensors.

Initially good working electrodes can be destroyed by contact with environmental samples [57]. Sudden potential changes, drift and the absence of response to concentration changes are the typical symptoms. This is probably caused by dissolution of hydrophobic substances from the biomass into the liquid membrane. If this occurs, often in cyanobacterial mats and dense environmental biofilms, a coating should be applied to protect the sensor from direct contact with the sample. A good separation is obtained by a thin (< 1 μm) layer of protein cross-linked by glutaraldehyde [35]. This coating is impermeable to the contaminants from the biomass, but smaller hydrophilic molecules can pass.

The selectivity is not affected. NO_2^- sensors become slower, while the response time of NO_3^-, pH and NH_4^+ sensors remains the same.

Finally, the shielding surrounding the sensor is filled with 0.3 mol L^{-1} KCl and connected with a silver wire to the reference. The filling electrolyte is connected with a chlorinated silver wire, by a coaxial cable to the voltmeter input. A voltmeter with high input impedance (10^{15} Ω) is needed. The resistance of the voltmeter must be at least 1000 times that of the microsensors, which have a resistance of 10^{10}–10^{12} Ω; therefore, a voltmeter used for measurements with macrosensors (input impedance < 10^{13} Ω) is unsuitable. The outer shielding of the coaxial cable must be positioned below the liquid shielding. The shielding is essentially a Faraday cage, but much more effective and convenient than a cage enveloping the whole equipment. A finished liquid membrane sensor is depicted in Figure 6.

The basic equipment for calibration and measurements consists of appropriate amplifiers and micromanipulators. Use of motorized micromanipulators is recommended to increase spatial resolution and to avoid vibrations by manual operation. A computer can be used for data collection and control of the motorized micromanipulator. A recorder should be used in parallel as it is helpful in recognizing occurrence of drift and slow response times.

2.3.3 Liquid Membrane Sensors for N Compounds

NH_4^+, NO_3^- and NO_2^- are the main compounds from the nitrogen cycle that can be measured by liquid membrane microsensors. NH_4^+ is released during

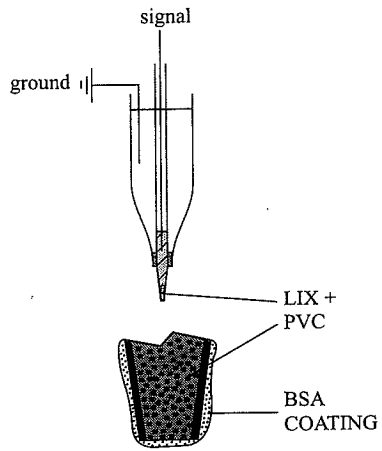

Figure 6. Scheme of a liquid membrane microsensor, with magnified tip. The BSA coating is a thin layer of cross-linked bovine serum albumin, the liquid membrane (LIX) is solidified with PVC

mineralization and oxidized by nitrification. NO_3^- is consumed mainly by denitrification and NO_2^- is an intermediate of both nitrification and denitrification. The low selectivity of liquid membrane sensors for NH_4^+ towards Na^+ and K^+ and of those for NO_3^- and NO_2^- towards Cl^-, prohibits measurements in seawater. Fortunately, NO_3^- can be measured in seawater with the recently developed biosensor [58]. However, for studies in freshwater, liquid membrane sensors may be preferred because of the ease of preparation.

The NH_4^+ electrode was developed first [29] and tested in studies of diffusion and reaction in enzymatic model systems. Since the measured profiles correlated well with those calculated with a diffusion–reaction model the electrode was considered reliable for profile measurements. The response time is ca. 1 s. The lifetime is approximately 1–2 d. The detection limit in distilled water is 1 μmol L^{-1}. The selectivity towards K^+ and Na^+ is low, so the sensor cannot be used in seawater. In most media the response is not log–linear below 10 μmol L^{-1}, but in freshwater systems, such as lake and river sediments and biofilms from waste water plants, the sensor can be used for measurements down to 1 μmol L^{-1}.

The later developed NO_3^- microsensor was also first tested in a model system, containing denitrifying bacteria [30]. The sensor is fast, with a t_{90} less than 1 s. Various liquid membrane chemistries have been used. The first NO_3^- sensor was based on the ion-exchanger from the Orion macroelectrode (1,10–phenanthroline nickel nitrate), and later other sensor chemistries were used in microsensors, such as methyltridodecylammonium nitrate, tricaprylylmethylammonium nitrate and tridodecylhexadecylammonium nitrate (Corning) [14]. Comparison of different microsensors showed that the nickel-based Orion liquid membrane had the best selectivity towards Cl^-, while the tridodecylhexadecylammonium-based sensor had the lowest detection limit. This comparison was made for plant physiology where Cl^- is the main interferent, although for microbial ecology studies the sensitivity towards hydrogen carbonate is more important [53]. Interfering substances are not very problematic when these are homogeneously distributed and thus present a constant background. Then they only increase the detection limit of the measurement. However, when the interfering compound is varying with depth one cannot subtract it as a constant background from the signal. In sediments and biofilms hydrogeno carbonate gradients are present, due to pH gradients and degradation of organic matter. Because of this problem NO_3^- did not seem to deplete in the denitrifying zones of sediments [53]. A comparison between different sensor chemistries showed that the Orion liquid membrane was much less sensitive towards hydrogeno carbonate than the liquid membrane used by Jensen (decyltrioctylammonium bromide and PVC in dibutyl phthalate, Radiometer) [55]. Indeed with microsensors based on the Orion liquid membrane the hydrogen carbonate interference is not a problem, and measurements showed that in denitrifying biofilms and sediments NO_3^- is depleted [30, 35, 59]. Therefore, the nickel-based Orion

compound is recommended for use in denitrifying systems, where determination of NO_3^- depletion is important. Regrettably, Orion has stopped this production, but a recipe is available [60]. Recently, a new sensor chemistry for NO_3^- microsensors has been developed [61]. The reported selectivities and detection limits exceed those of the Orion liquid membrane, but it has not yet been used in ecological studies. A disadvantage of this sensor is its sensitivity towards sulfide, which irreversibly poisons the sensor. Sulfide also affects the signal of sensors with the nickel-based liquid membrane, although not irreversibly. Most NO_3^- liquid membranes have a detection limit in distilled water of 10 μmol L^{-1}, but measurements can be made down to 1 μmol L^{-1} (using the Orion liquid membrane). Surprisingly, NO_3^- microsensors coated with cross-linked BSA have a lower detection limit (1 μmol L^{-1} in interferent-free water) than uncoated sensors. The lifetime of the sensors is ca. 5 h, and 8–12 h when the liquid membrane is gelled with PVC.

The most recent development was the NO_2^- microsensor [35], which was applied in nitrifying and denitrifying biofilms. This carrier-based sensor is highly selective for NO_2^-, as can be appreciated from Table 1. The response of this sensor is strongly size dependent: the performance of microsensors with 1–2 μm tips is too poor, with respect to selectivity and detection limit, for practical use [45]. This is probably a wall effect as excellent sensors are obtained when the tip size is 10–20 μm. When stored dry, this sensor can be used for weeks. The response time is concentration dependent: in the range of 100–1000 μmol L^{-1} it is 1 s, from 1–100 μmol L^{-1} it is ca. 10–15 s, and below 1 μmol L^{-1} it increases significantly to minutes. The detection limit in distilled water is in the sub μmol L^{-1} range, and a log–linear response can be obtained down to 10^{-8} mol L^{-1}. In seawater the detection limit is 10 μmol L^{-1}, below which the response curve tapers off sharply. A serious problem with this sensor is its sensitivity towards sulfide and other reduced sulfur compounds, that reduce the Co(III) in the carrier molecule. The poisoning is irreversible, and results in a continuous drift. This phenomenon is a major drawback, as it may prohibit measurements in anoxic zones. Poisoning was observed in sulfate reducing biofilms, at depths where sulfide was detected (data not shown). However, also in anoxic zones of freshwater sediments, where no sulfide was detected, poisoning occurred, probably by reduced sulfide species not detected by the sulfide microsensors (data not shown). The recently developed new NO_2^- carrier may not have this problem.

2.3.4 Ca^{2+} Microsensors

Ca^{2+} sensors were developed for animal physiology and as ultra-microelectrodes (< 1 μm) are often used for intracellular studies. They are useful in this field because of their extremely low detection limit. Several carriers are available, with different detection limits (0.1 nmol L^{-1} – 0.1 μmol L^{-1}), selectivities

and response times (1–5 s). The actual response times are probably less than 200 ms [61], but cannot be determined accurately because of the slow mixing of calibration solutions [2]. For environmental studies all are suitable, as the concentrations are measured in the $\mu mol\,L^{-1}$ to $mmol\,L^{-1}$ range instead of the $nmol\,L^{-1}$ range. The sensors for Ca^{2+} are, together with those for H^+, the best liquid membrane sensors available. The selectivity allows measurements in marine and hypersaline conditions.

2.3.5 Comparison of Liquid Membrane with Other Microsensors

Except for pH, liquid membrane sensors measure a unique range of compounds, making true comparison difficult. In general, both the signal stability and lifetime of liquid membrane microsensors are poor compared with those of full glass, amperometric O_2 and H_2S, and optical microsensors. Typically, liquid membrane sensors can be used for a few days, after which the detection limit is too high or the calibration levels off (slope factor k decreases). Especially when a low detection limit is important, freshly-prepared sensors should be used. Also the signal drifts, usually $0.5–2\,mV\,h^{-1}$, resulting in an error of $2–7.5\%\ h^{-1}$ for monovalent ions. Drift is caused by hydration of the microcapillaries and degradation of the liquid membrane. NO_3^- sensors last less than 1 d, because the nickel complex is slightly water soluble and disappears from the membrane. NH_4^+ and proton carriers are much more hydrophobic and these microsensors last for a few days to 1 week, when stored dry between measurements. NO_2^- sensors can be stored for weeks. For comparison, drift of amperometric O_2 [26] and H_2S [34] microsensors is a few % per day, and for microoptrodes, it is in the order of a few % per month; pH glass microsensors do not significantly drift during 1 week. The lifetime of microsensors is ca. 1 month (amperometric H_2S), half a year (amperometric O_2) or more than a year (optrodes and full glass pH sensors).

This comparison is unfavorable for liquid membrane sensors, but they do have their positive sides. For NH_4^+, NO_2^- and Ca^{2+} no alternative sensors exist. The biosensor [58] (see also Chapter 4) does not distinguish between NO_2^- and NO_3^-. Drift can be determined between experiments by calibrations or by determining the signal in the bulk liquid, which usually has a constant composition. Since drift is constant, the signal can simply be corrected. Liquid membrane sensors are easy and fast to prepare, which partially compensates for their short lifetime. The reported damage by contact with biomass [57] can be prevented by a hydrophilic coating. Their small size and absence of substrate consumption may be crucial for some applications. For example, the small size of pH liquid membrane sensors is essential for the functioning of fast, small ($< 10\,\mu m$ tip) and sensitive CO_2 microsensors [6]. Full glass pH sensors are too large for this purpose and no functioning microsensors could be made. Also the full glass pH sensors may have insufficient spatial resolution in highly active

systems. The NO_3^- biosensor has a tip size of $20\,\mu m$, which may disturb the matrix structure and profiles in highly active systems with steep gradients. Thus for highly active biofilms, liquid membrane microsensors may be a better choice. In conclusion it can be stated that, despite their disadvantages, liquid membrane microsensors are highly useful tools for microprofiling of nitrogen species in freshwater systems and for measurements of pH and Ca^{2+} in all aquatic environments.

3 ECO-PHYSIOLOGICAL STUDIES WITH LIQUID MEMBRANE SENSORS

Microsensors are ideal tools for fundamental studies on microbial processes in sediments and biofilms. Most commonly used is the O_2 microsensor, while only a limited number of research groups have worked with liquid membrane electrodes. Examples of studies using liquid membrane sensors on the nitrogen cycle, with emphasis on nitrification and denitrification, will be given (see Table 3 for an extensive overview). NO_3^- and NH_4^+ liquid membrane sensors have also been used for plant physiological studies, i.e. in uptake in roots, but this application will not be reviewed here. Secondly, some applications of the Ca^{2+} microsensor in environmental research will be shown.

Concentration profiles are a result of conversions and mass transport. In most sediments and biofilms transport of substrate and product takes place by diffusion. Consequently, if the diffusion coefficients are known, local conversion rates can be derived. This is demonstrated in Figure 7, which schematically shows substrate and product profiles occurring during nitrification and denitrification. As a result of nitrification NH_4^+ will decrease in the nitrifying zone, usually determined by the O_2 penetration depth, and in the same zone NO_3^- will increase. Because of denitrification NO_3^- will decrease in the anoxic zones. In layers where consumption and production occurs the profiles of the respective compounds are curved. From the profiles, NH_4^+ and NO_3^- fluxes can be determined using Fick's law ($J = D\,dc/dx$), at different depths in the sediment. Then the volumetric conversion rates can be determined in a layer of interest, by subtracting the fluxes at the top and the bottom of that layer and dividing this number through the thickness of the layer (see Figure 13). If the concentration profiles are recorded at sufficient spatial resolution, a fine scale distribution of activity can be determined [71]. Alternatively, one can use a reaction–diffusion model to calculate the profiles and by an iterative procedure fit the modeled profiles to those measured. In such a procedure the activity profile is changed until a good fit is obtained [29,30,70,76].

Table 3. Overview of *in situ* studies with microsensors

Subject	Microsensors	Metabolic activity	Goal	References
aggregates	NO_3^-, NH_4^+, O_2, pH	nitrification	distribution activity	62
aggregates	NO_3^-, NO_2^-, NH_4^+, O_2, pH	nitrification	distribution activity and microbial species	63
biofilm	NO_3^-, NH_4^+, O_2	nitrification, aerobic mineralization	distribution activity; effect of conditions	64
biofilm	NO_3^-, NO_2^-, NH_4^+, O_2, H_2S	denitrification, sulfate reduction, sulfide oxidation, aerobic mineralization	distribution activities; anaerobic sulfide oxidation	65
biofilm	NO_3^-, NO_2^-, NH_4^+, O_2, flow	nitrification, denitrification, flow, aerobic mineralization	distribution activity	35
biofilm	NO_3^-, NO_2^-, NH_4^+, O_2	nitrification, denitrification, flow, aerobic mineralization	distribution activity; distribution of microbial species; development of biofilm	63, 66
activated sludge	NO_3^-, NO_2^-, NH_4^+, O_2	nitrification, denitrification, aerobic mineralization	anoxic processes in aerated sludge	67
Beggiatoa mat	NO_3^-, O_2	denitrification	interfacial fluxes	59, 68, 69
sediment	NO_3^-, NH_4^+, O_2	nitrification, denitrification, aerobic mineralization	distribution activities	17, 30, 59, 69
sediment	NO_3^-, O_2	nitrification, denitrification, aerobic mineralization	regulation and distribution of activities	53, 70
sediment	NO_3^-, NH_4^+, O_2	nitrification, denitrification, aerobic mineralization, photosynthesis	distribution of activities; effect of photosynthesis of benthic algae on nitrification and denitrification	71
sediment	NO_3^-, NH_4^+, O_2	nitrification, denitrification	distribution activities; effect of plants roots on nitrification and denitrification	72
sediment	Ca^{2+}	calcium precipitation	effect of photosynthesis by benthic algae	73
Chara corallina	Ca^{2+}, pH	calcification	Ca^{2+}, H^+ uptake	74, 75

3.1 STUDIES ON THE N-CYCLE IN BIOFILMS

Most information on a process is obtained if all reactants are determined; therefore, results from a combination of sensors are most informative. Such a study was first performed on nitrifying aggregates from a fluidized bed reactor [62]. The reactor was fed with a mineral medium; therefore, nitrification was the main process (besides some heterotrophic growth on decaying nitrifiers). At that time the NO_2^- microsensor was not yet developed, so only NH_4^+, NO_3^-

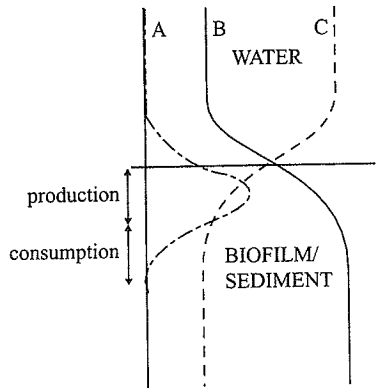

Figure 7. Schematic representation of substrate (C), end product (B) and intermediate product (A) profiles. The intermediate is produced in the top of the biofilm or sediment and consumed in the deeper zone. Such profiles can be found in nitrifying/denitrifying systems, where nitrate is formed in the upper oxic zone and consumed in the anoxic zone. The zones of production and consumption of the intermediate are indicated by arrows

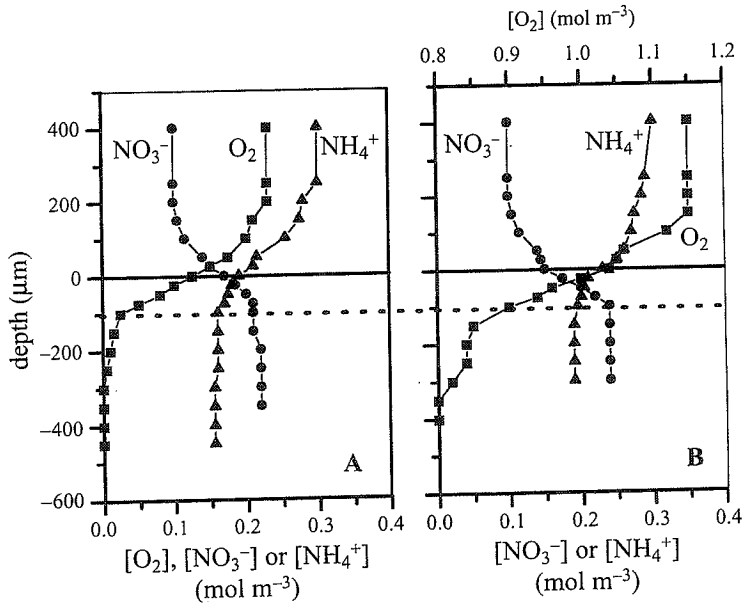

Figure 8. NH_4^+ (▲), NO_3^-(●) and O_2(■) profiles in a nitrifying aggregate under aeration (A) and during sparging with pure oxygen (B). Depth = 0 indicates the aggregate surface, negative values indicate positions inside the aggregate. The dotted line indicates the boundary of the nitrifying zone [62]

and O_2 profiles were measured (see Figure 8). If incubated under normally aerated conditions (A), O_2 penetrated the outer 100 μm of the aggregates, and NH_4^+, NO_3^- and O_2 fluxes were close to the stoichiometry of NH_4^+ oxidation to NO_3^-. At higher concentrations (B), O_2 penetrated the whole aggregate, but the NO_3^- and NH_4^+ profiles remained unchanged. It was concluded that the nitrifying organisms were predominantly located in the outer layer of 100 μm thickness, the center of the 2 mm sized aggregates was inactive. For the NO_3^- microsensors the Orion liquid ion exchanger (LIX) was used. In these measurements hydrogen carbonate interference could not become a problem as in this autotrophic system no hydrogen carbonate production occurred.

A later study on the same reactor showed similar NH_4^+, NO_3^- and O_2 profiles. Now also NO_2^- was measured, and found to be present in insignificant amounts (< 10 μmol L^{-1}) under reactor conditions [63]. This study was combined with molecular analysis of the nitrifying population, to determine the dominant species and their distribution. Interestingly, no *Nitrobacter* or *Nitrosomonas* could be detected, the species most commonly found in nitrifying systems with microbial cultivation techniques. A more detailed analysis, by cloning and sequencing 16S rDNA, showed the presence of a consortium of new *Nitrospira* and *Nitrosospira* species. *In situ* hybridization with 16S rRNA probes, designed using the sequences found, showed that the two types of cells formed separate dense clusters that were in close contact with each other. It was hypothesized that *Nitrobacter* and *Nitrosomonas* strains are adapted to high substrate concentrations, which explains their occurrence in enrichment cultures. *Nitrospira* and *Nitrosospira* can compete under low NH_4^+ and NO_2^- concentrations as present in most natural environments. These species may well be more relevant nitrifiers than *Nitrobacter* and *Nitrosomonas*, and kinetic parameters derived from *Nitrobacter* and *Nitrosomonas* may not be useful to describe nitrification in nature and waste water treatment. Very recently activity profiles measured with microsensors were combined with specific cell counts by *in situ* hybridization, resulting in specific activities (i.e. conversion rates per cell). The results confirmed that *Nitrospira* and *Nitrosospira* have a much higher substrate affinity than *Nitrobacter* and *Nitrosomonas* [60].

Similar microsensor studies were performed on flat biofilms from a laboratory reactor [64]. Also these researchers showed that in a nitrifying biofilm most of the nitrifying activity was present in the outer 100–200 μm (see Figure 9). In this autotrophic biofilm no short term effects of glucose addition were observed, demonstrating the absence of a heterotrophic population. In a biofilm grown in a medium amended with organics both nitrification and aerobic mineralization of organics occurred. The NH_4^+ and NO_3^- profiles indicated that in this mixed heterotrophic–autotrophic biofilm nitrification was inhibited by addition of glucose, owing to competition for O_2 by the heterotrophic population. Strangely, no denitrification was observed, as NO_3^- concentrations in the anoxic zone were equal to that in the oxic zone. The NO_3^- measurements

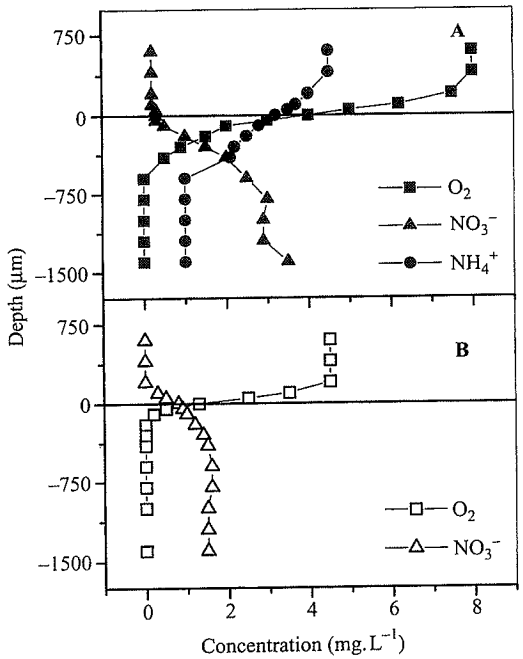

Figure 9. (A) NH_4^+, NO_3^- and O_2 profiles in a nitrifying biofilm without addition of glucose; (B) NO_3^- and O_2 profiles in the same biofilm, but with addition of glucose. Addition of glucose (80 mg L^{-1}) reduced the nitrification, probably because of competition for oxygen between heterotrophic and nitrifying populations. Glucose addition did not lead to denitrification, which would have resulted in nitrate decrease or depletion in the anoxic zone. Depth = 0 indicates the aggregate surface, negative values indicate positions outside the aggregate. Reproduced from ref. [64]

were performed with microsensors based on the Orion LIX. These researchers did not mention any technical problems with microsensors.

The effect of NO_3^- addition on sulfide profiles was investigated in a 2 cm thick biofilm obtained from the wall of a waste water plant (Figure 10) [35, 65]. In absence of NO_3^- the O_2 profile overlapped with the sulfide profile, indicating the aerobic oxidation of sulfide. Addition of nitrate resulted in a separation of the sulfide and O_2 profiles as shown previously [16], indicating anaerobic sulfide oxidation. NO_3^- (measured with an Orion LIX microsensor) penetrated the biofilm deeper (to 250 μm) than O_2 (to 150 μm) and overlapped with the sulfide profile. No HCO_3^- interference was noticed as measurements showed complete NO_3^- depletion. In the denitrifying zone a significant NO_2^- peak was observed, so that both NO_2^- and NO_3^- could be terminal electron acceptors for sulfide oxidation. In contrast with hydrogeno carbonate, sulfide did cause

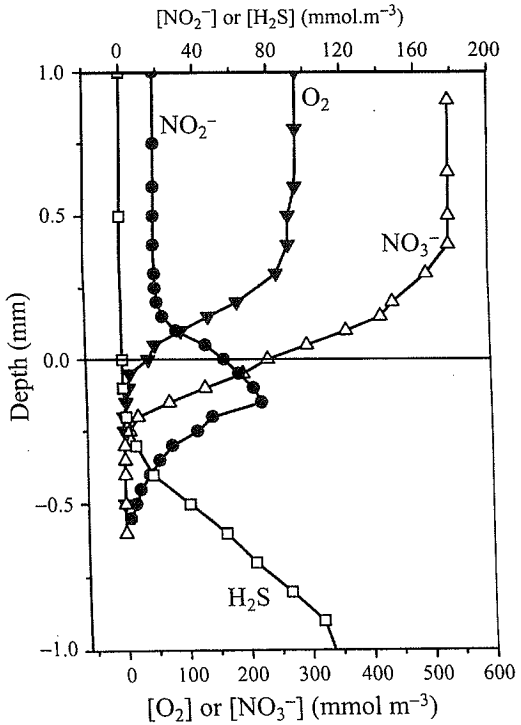

Figure 10. NO_3^-(Δ), NO_2^-(●), H_2S(□) and O_2 (▲) profiles in a thick biofilm from a wastewater treatment plant. In absence of NO_3^-, H_2S and O_2 profiles overlapped, indicating aerobic sulfide oxidation (not shown). After addition of nitrate the H_2S and O_2 profiles separated, indicative of anaerobic sulfide oxidation, with either NO_3^- or NO_2^- as e-acceptor

serious interference. At a concentration of more than 50 μmol L^{-1} sulfide, drift of both NO_3^- and NO_2^- sensors made further profiling impossible. However, meaningful profiles could be recorded as both NO_2^- and NO_3^- were depleted before the interference became a problem.

The studies mentioned above were performed on biofilms and aggregates placed in flowcells specially designed for microsensor studies, i.e. in samples removed from the reactor in which they were grown. With the shielded sensors *in situ* measurements can be done, inside an operating reactor. An example is a study on a biofilm from a membrane reactor, in which both nitrification and denitrification occurred simultaneously [35]. The biofilm was growing on a silicon tubing pressurized with 3 atm air. O_2 diffused through the silicon tube ca. 300 μm deep into the base of the 2.5 mm thick biofilm. NH_4^+ and organics were supplied from the bulk phase. NH_4^+ was consumed in the oxic zone, and

converted to NO_3^-. In this nitrifying zone a peak of NO_2^- was observed. NO_2^- and NO_3^- were consumed in the anoxic zone, owing to denitrification. In this reactor the development of a nitrifying biofilm occurred in ca. 2 months. Nitrification was not complete and NO_2^- was the main product. After switching to heterotrophic conditions denitrification started within a few hours. Initially NO_2^- consumption was located in patches but after 2 weeks a homogeneous anoxic denitrifying layer covered the nitrifying base film [66].

3.2 STUDIES ON THE N-CYCLE IN SEDIMENTS

The first studies with liquid membrane sensors for NH_4^+ and NO_3^-, combined with O_2 profiles, were performed in sandy and silty sediments from a meso-eutrophic lake (see Figures 11 and 12) [17, 59]. In both types of sediment NH_4^+ oxidation occurred in the aerobic zone, and denitrification in the anaerobic zone. Conversion rates were calculated from the profiles, showing that in organic-rich, silty sediments both nitrification and denitrification were more intense than in sandy sediments that were low in organics. The NO_3^- measurements were performed with the Orion LIX, and no hydrogen carbonate interference was found. A problem in the profiling of sandy sediments was irregularities in the signal due to collisions with sand grains. Therefore, the profiles with liquid membrane sensors were recorded while retracting the microsensor out of the sediment.

At the surface of sulfide-rich sediments sulfur bacteria from the genus *Beggiatoa* often grow abundantly in white mats. Most *Beggiatoa* species cannot be cultivated, so little is known about their metabolic activities. A study on semi-purified mats was performed with NO_3^- microsensors [68]. *Beggiatoa* mats were

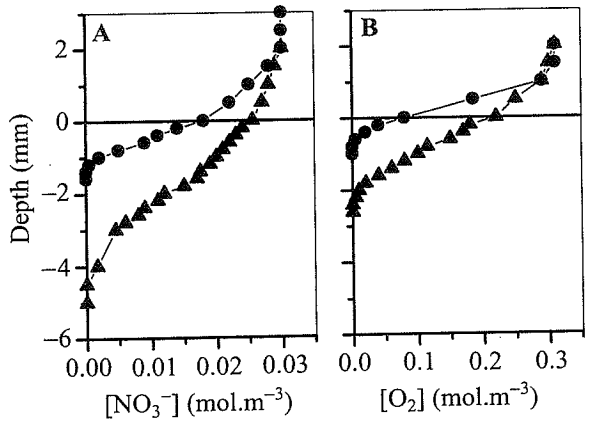

Figure 11. NO_3^- and O_2 profiles in sediments from a lake. Profiles in organic rich silt (●) and sand (▲). In both sediments, nitrate penetrates deeper than oxygen

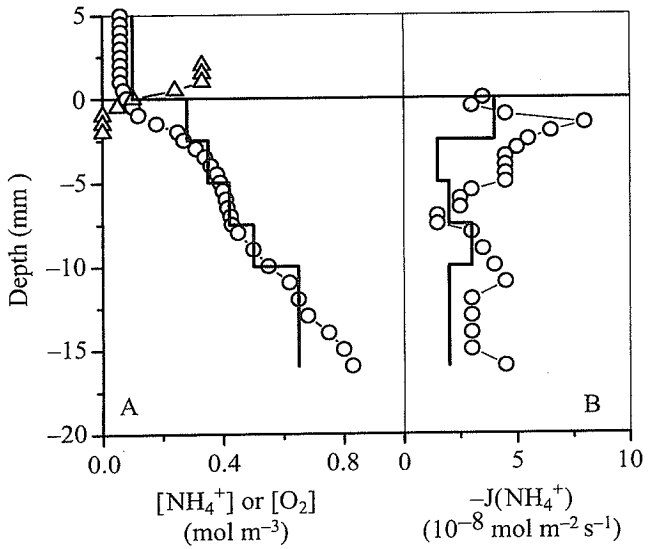

Figure 12. NH_4^+(○) and O_2(△) profiles (A), and the corresponding fluxes, J (B), in the same silty sediments as in Figure 11. The block diagrams indicate ammonium concentrations measured by porewater extraction

removed from a sediment surface and washed carefully with sterile water until no bacteria other than *Beggiatoa* were present. After a 1 h incubation in natural lake water these mats were profiled and found to consume nitrate at very high rates. Oxygen did not penetrate more than 10 μm in the mats. This led to the conclusion that these organisms are efficient denitrifiers and because of their abundance may have significant effects on the nitrogen budgets in aquatic systems. Recent insights make it much more likely that these organisms do not denitrify, but ammonify (conversion of NO_3^- to NH_4^+ instead of N_2).

Two later studies in model sediment, from which the burrowing animals were removed, were done with NO_3^- and O_2 microsensors [53, 70]. The effect of O_2 and NO_3^- concentration in the overlying water on the localization of nitrification and denitrification was determined, by fitting the NO_3^- profiles with a diffusion–reaction model. Also in this research denitrification was exclusively found in the anaerobic zone. At increasing O_2 concentrations, nitrification in the sediment became a more important NO_3^- source for denitrification than the bulk liquid, owing to increased path length for NO_3^- diffusion from the bulk to the anoxic zone. Secondly, at high O_2 concentrations nitrification was localized in the lower parts of the aerobic zones, adjacent to the anaerobic zones. It was hypothesized that NH_4^+ then became limiting for nitrification. Unfortunately, NH_4^+ was not measured in these studies. The serious problems due to hydrogen carbonate interference, as reported in these studies, can be attributed to the

choice of LIX chemistry (Radiometer). These researchers introduced the shielding surrounding the liquid membrane sensor to protect the signal from noise. This was an important improvement, that made the use of a Faraday cage obsolete.

Photosynthesizing benthic algae can have a strong effect on the nitrogen cycle, as shown in a study with NH_4^+, NO_3^- and O_2 microsensors (Figure 13) [71]. In a freshwater sediment containing benthic algae, illumination increased the O_2 penetration depth. This stimulated nitrification, and thus the NH_4^+ profile developed a dip and NO_3^- formed a peak in the aerobic zone. NO_3^- diffused both downwards into the anaerobic zone, where it was used by denitrification, and upwards to the sediment surface where it was consumed, most likely by the benthic algae. Thus it was possible to visualize with microsensors part of the N-cycle in sediments: NH_4^+ was formed in the deeper sediments by mineralization, diffused upwards into the nitrification zone, was converted to NO_3^-, which was partially used in denitrification and partially incorporated in algal biomass, which after mineralization will again contribute to the NH_4^+ pool.

Recently it was shown, using a combination of ^{15}N isotope pairing and microsensor techniques (O_2, NO_3^- and NH_4^+), how plants enhance nitrification and denitrification activity in sediments [72]. Microprofiles showed that O_2

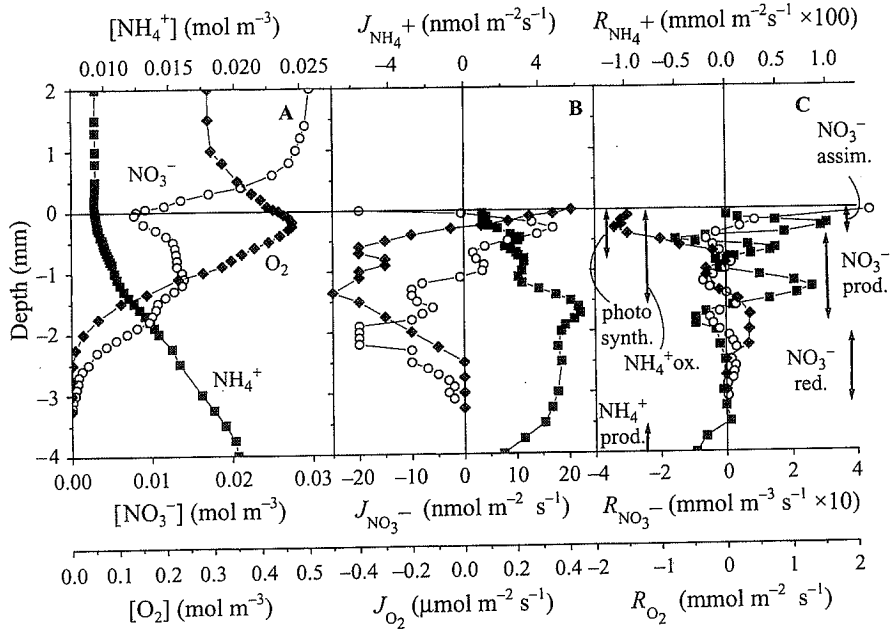

Figure 13. The distribution of NO_3^-(○), O_2(◆) and NH_4^+(■) in a lake sediment during light incubation. From the concentration profiles (A), the local fluxes, J, were calculated (B) and from these the local conversion rates, R, (C)

diffused out of the roots, and that in a nitrifying zone adjacent to the roots NH_4^+ was consumed and NO_3^- was formed. Illumination increased the O_2 content of the sediment and stimulated nitrification. The root-associated nitrifying zone was surrounded by zones of denitrification, leading to a close coupling between nitrification and denitrification. No problems with microsensors were reported in this study.

3.3 ECO-PHYSIOLOGICAL MEASUREMENTS WITH Ca^{2+} SENSORS

The Ca^{2+} sensor is widely used in the field of animal physiology. Since calcium is involved in a large number of biological and biogeochemical processes, it is surprising that this sensor has been used so rarely in aquatic studies.

Photosynthesis is an important regulating mechanism of calcification. The CO_2 fixation by photosynthesis and concomitant pH increase can lead to oversaturation of $CaCO_3$ and thus stimulate its precipitation. If precipitation rates equal photosynthesis no net CO_2 is consumed and the pH remains constant. Ca^{2+} microprofiles were recorded in a freshwater algal film [73] and Ca^{2+} fluxes were calculated from 0.5–1.3 $\times 10^{-6}$ mol m^{-2} s^{-1}. In this study photosynthesis was not determined. Other studies [33,77] have reported photosynthesis rates of ca. 3×10^{-6} mol m^{-2} s^{-1} for sediments with benthic algae, which is in the same order of magnitude as the Ca^{2+} fluxes. More detailed measurements are needed to clarify the relation between photosynthesis, water chemistry and calcification in algal mats.

Elegant studies have been done on the giant cell alga *Chara corallina* [74,75]. This alga has a calcification to photosynthesis ratio of 1. Calcification is confined to distinct bands around the stem. Protons generated by calcification are transported to the cell surface in between calcifying bands. Locally the pH is lowered and the carbonate system shifted towards CO_2 which is taken up for photosynthesis. Microsensors for pH and Ca^{2+} were positioned at the cell surface and the cells were subjected to light–dark shifts. These measurements indicated that Ca^{2+} is excreted at calcifying sites in exchange for H^+, while Ca^{2+} is taken up in between calcifying bands. By this mechanism calcification is regulated by the alga, and can be fine-tuned to the photosynthesis, independent of the Ca^{2+} concentration in the water.

Due to the signal stability, the Ca^{2+} sensor can be used to detect small changes in environments with a large background concentration. For example, it is possible to measure concentration changes of the order of a few μmol L^{-1} in seawater, which has a concentration of ca. 8 mmol L^{-1}. In the sea, at depths of less than ca. 4000 m, calcium carbonate is oversaturated, and thus can precipitate. Marine organisms have to regulate the calcium precipitation carefully, in order not to get encrusted. Corals are probably the most spectacular calcifying systems. Despite this, the regulation of calcification in corals is poorly understood. With a combination of microsensors (H^+, O_2, CO_2 and Ca^{2+}) the

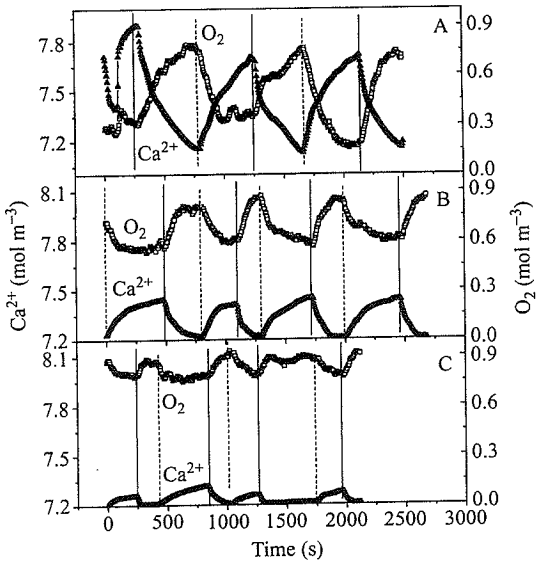

Figure 14. Ca^{2+}(▲) and O_2(□) dynamics at the surface of a coral induced by light–dark shifts, measured at 510 (A), 230 (B) and 70 (C) μmol photons m^{-2} s^{-1}. The simultaneous response, similar initial rates and amplitude of the dynamics indicate a close coupling

relation between calcification and photosynthesis in corals [78] and foraminifera [79] is currently being studied in our laboratory. In Figure 14 the effect of light–dark shifts in the O_2 and Ca^{2+} dynamics at the surface of coral tissue is shown. Since both the amplitude and the initial rates of the dynamics are similar, processes regulating O_2 and Ca^{2+} concentrations at the surface seem to be coupled. Indeed, a direct relation between calcium uptake and the activity of the photosynthetic apparatus could be demonstrated. Such a coupling could not be shown between the dynamics of CO_2 or H^+ and Ca^{2+}. Results of the measurements are promising and publications can be expected soon.

4 OUTLOOK

Although potentiometric analysis has been an established technique for decades, new developments also continue in this field. These developments sooner or later reach the level of microsensors, where these inventions can be used for eco-physiological, environmental and diagenetic studies. Interesting is the finding of new ionophores that may lead to improved or new sensors. Hopefully, the new nitrite ionophore will not be poisoned by sulfide. The reported finding

of a sulfate ionophore may lead to new possibilities in detection of sulfate reduction.

Furthermore new detection techniques are under development for measurement of trace metals. Ion-sensitive electrodes have detection limits in the $\mu mol\,L^{-1}$ range, unsuitably high for trace metals. It was shown that this was determined by leaking of analyte ions from the internal electrolyte through the membrane [80]. By choosing an electrolyte that buffers the analyte ion at a low concentration, detection limits could be reduced down to the $pmol\,L^{-1}$ range [81]. This, together with the development of new highly selective ionophores for heavy metals [3,44] may open perspectives for the analysis of trace metals by potentiometric methods.

REFERENCES

1. Skoog, D. A. and Leary, J. (1992). *Principles of Instrumental Analysis*, 4th edn, Saunders College Publishing, Fort Worth.
2. Ammann, D., Bührer, T., Schefer, U., Müller, M. and Simon, W. (1987). Intracellular neutral carrier based Ca^{2+} microelectrode with sub-nanomolar detection limit, *Pflügers Arch.*, **409**, 223.
3. Pineros, M. A., Shaff, J. E. and Kochian, L. V. (1998). Development, characterization, and application of a cadmium-selective microelectrode for the measurement of cadmium fluxes in roots of *Thlaspi* species and wheat, *Plant Physiol.*, **116**, 1393.
4. Midorikawa, T., Tanoue, E. and Sugimura, Y. (1990). Determination of complexing ability of natural ligands in seawater for various metal ions using ion selective electrodes, *Anal. Chem.*, **62**, 1737.
5. Lake, D. L., Kirk, P. W. W. and Lester, J. N. (1989). Heavy metal solids association in sewage sludges, *Wat. Res.*, **23**, 285.
6. De Beer, D., Glud, A., Epping, E. and Kühl, M. (1997). A fast responding CO_2 micro-electrode for profiling sediments, microbial mats and biofilms, *Limnol. Oceanogr.*, **42**, 1590.
7. Cai, W. J. and Reimers, C. E. (1993). The development of pH and pCO_2 microelectrodes for studying the carbonate of pore waters near the sediment–water interface, *Limnol. Oceanogr.*, **38**, 1762.
8. Westcott, C. C. (1978). *pH Measurements*, Academic Press, San Diego.
9. Oesch, U., Ammann, D. and Simon, W. (1986). Ion-selective membrane electrodes for clinical use, *Clin. Chem.*, **32**, 1448.
10. Müller, M., Rouilly, M., Rustenholz, B., Maj-Zurawska, M. Z. H. and Simon, W. (1988). Magnesium selective electrodes for blood serum studies and water hardness measurement, *Mikrochim. Acta*, **3**, 283.
11. Kessler, M. (1976). *Ion and Enzyme Electrodes in Biology and Medicine*, Urban & Schwarzenberg, Munich.
12. Scholer, R. P. and Simon, W. (1970). Antibiotika-Membranelektrode zur selektiven Erfassung von Ammoniumionenaktivitäten, *Chimia*, **24**, 372.
13. Stepanek, R., Krautler, B., Schulthess, P., Lindemann, B., Ammann, D. and Simon, W. (1986). Aquocyanocobalt(III)-hepta(2–phenylethyl)-cobyrinate as a cationic carrier for nitrite-selective liquid-membrane electrodes, *Anal. Chim. Acta*, **182**, 83.

14. Zhen, R.-G., Smith, S. J. and Miller, A. J. (1992). A comparison of nitrate-selective microelectrodes made with different nitrate sensors and the measuremets of intracellular nitrate activities in cells of excised barley roots, *J. Exp. Botany*, **43**, 131.
15. Carey, C. M. and Riggan, W. B. (1994). Cyclic polyamine ionophore for use in a dibasic phosphate-selective electrode, *Anal. Chem.*, **66**, 3587.
16. Kühl, M. and Jørgensen, B. B. (1992). Microsensor measurements of sulfate reduction and sulfide oxidation in compact microbial communities of aerobic biofilms, *Appl. Environ. Microbiol.*, **58**, 1164.
17. De Beer, D., Sweerts, J.-P. R. A. and van den Heuvel, J. C. (1991). Microelectrode measurement of ammonium profiles in freshwater sediments, *FEMS Microbiol. Ecol.*, **86**, 1.
18. Bakker, E., Bühlmann, P. and Pretsch, E. (1997). Carrier based ion-selective electrodes and bulk optodes. 1. General characteristics, *Chem. Rev.*, **97**, 3083.
19. Ammann, D. (1986). *Ion-selective Microelectrodes: Principles, Design and Applications*, Springer, Berlin.
20. Albanese, R. A. (1973). On microelectrode distortion of tissue oxygen tensions, *J. Theor. Biol.*, **38**, 143.
21. Zhang, T. C. and Bishop, P. L. (1994). Evaluation of tortuosity factors and effective diffusivities in biofilms, *Wat. Res.*, **5**, 2279.
22. Muller, W., Winnefeld, A., Kohls, O., Scheper, T., Zimelda, W. and Baumgartl, H. (1994). Real and pseudo oxygen gradients in Ca-alginate beads monitored during polarographic pO_2–measurements using Pt-needle microelectrodes, *Biotechnol. Bioeng*, **44**, 617.
23. Glud, R. N., Gundersen, J. K., Revsbech, N. P. and Jørgensen, B. B. (1994). Effects on the benthic diffusive boundary layer imposed by microelectrodes, *Limnol. Oceanogr.*, **39**, 462.
24. Bungay, H. R., Whalen, W. J. and Sanders, W. M. (1969). Microprobe techniques for determining diffusivities and respiration rates in microbial slimes, *Biotechnol. and Bioeng.*, **11**, 765.
25. Revsbech, N. P. and Ward, D. M. (1983). Oxygen microelectrode that is insensitive to medium chemical composition: Use in an acid microbial mat dominated by *Cyanidium caldarum*, *Appl. Environ. Microbiol.*, **45**, 755.
26. Revsbech, N. P. (1989). An oxygen microelectrode with a guard cathode, *Limnol. Oceanogr.*, **55**, 1907.
27. Revsbech, N. P., Nielsen, L. P., Christensen, P. B. and Sorensen, J. (1988). A combined oxygen and nitrous oxide microsensor for denitrification studies, *Appl. Environ. Microbiol.*, **45**, 2245.
28. Hinke, J. (1969). Glass microelectrodes for the study of binding and compartmentalisation of intracellular ions. In *Glass Microelectrodes*, ed. Lavallee, M., Schanne, O. F. and Herbert, N. C., John Wiley & Sons, New York, p. 349.
29. De Beer, D. and Van den Heuvel, J. C. (1988). Response of ammonium-selective microelectrodes based on the neutral carrier nonactin, *Talanta*, **35**, 728.
30. De Beer, D. and Sweerts, J. P. R. A. (1989). Measurements of nitrate gradients with an ion-selective microelectrode, *Anal. Chim. Acta*, **219**, 351.
31. Larsen, L. H., Revsbech, N. and Binnerup, S. J. (1996). A microsensor for nitrate based on immobilized denitrifying bacteria, *Appl. Environ. Microbiol.*, **62**, 148.
32. Larsen, L. H., Kjaer, T. and Revsbech, N. P. (1997). A microscale NO_3^- biosensor for environmental applications, *Anal. Chem.*, **69**, 3527.
33. Revsbech, N. P., Jørgensen, B. B., Blackburn, T. H. and Cohen, Y. (1983). Microelectrode studies of the photosynthesis and O_2, H_2S and pH profiles of a microbial mat, *Limnol. Oceanogr.*, **28**, 1062.

34. Jeroschewski, P., Steukart, C. and Kühl, M. (1996). An amperometric microsensor for the determination of H_2S in aquatic environments, *Anal. Chem.*, **68**, 4351.
35. De Beer, D., Schramm, A., Santegoeds, C. M. and Kühl, M. (1997). A nitrite microsensor for profiling environmental biofilms, *Appl. Environ. Microbiol.*, **63**, 973.
36. Damgaard, L. R. and Revsbech, N. P. (1997). A microscale biosensor for methane, *Anal. Chem.*, **69**, 2262.
37. Tercier, M. L., Parthasarathy, N. and Buffle, J. (1995). Reproducible, reliable and rugged Hg-plated Ir-based microelectrode for in situ measurement in natural waters, *Electroanalysis*, **7**, 55.
38. Awasthi, S. P. (1990). *Ion-selective Electrodes—a Review*, World Scientific, Singapore.
39. Thomas, R. C. (1978). *Ion-sensitive Intracellular Microelectrodes, How to Make and Use Them*, Academic Press, London.
40. Revsbech, N. P. and Jørgensen, B. B. (1986). Microelectrodes: their use in microbial ecology, *Adv. Microbial Ecol.*, **9**, 293.
41. Stefanac, Z. and Simon, W. (1967). Ion specific electrochemical behaviour of macrotetrolides in membranes, *Microchem. J.*, **12**, 125.
42. Walker, J. L. (1971). Ion specific liquid ion exchanger microelectrodes, *Anal. Chem.*, **43**, 89.
43. Morf, W. E. and Simon, W. (1978). *Ion-selective Electrodes Based on Neutral Carriers*, Plenum, New York.
44. Bühlmann, P., Pretsch, E. and Bakker, E. (1998). Carrier based ion-selective electrodes and bulk optodes, *Chem. Rev.*, **98**, 1593.
45. Schaller, U., Bakker, E., Spichiger, U. and Pretsch, E. (1994). Nitrite selective microelectrodes, *Talanta*, **41**, 1001.
46. Schulthess, P., Shijo, Y., Pham, H. V., Pretsch, E., Ammann, D. and Simon, W. (1981). A hydrogen ion-selective liquid-membrane electrode based on tri-n-dodecylamine as neutral carrier, *Anal. Chim. Acta*, **131**, 111.
47. Khuri, R. N., Bogharian, K. K. and Agulian, S. K. (1974). Intracellular bicarbonate in single skeletal muscle fibers, *Pflügers Arch.*, **349**, 285.
48. Munoz, J. L., Deymhimi, F. and Coles, J. A. (1983). Silanization of glass in the making of ion-selective microelectrodes:, *J. Neurosci. Methods*, **8**, 231.
49. Ammann, D., Lanter, F., Steiner, R. A., Schulthess, P., Shio, Y. and Simon, W. (1981). Neutral carrier based hydrogen-ion selective microsensor for extra- and intracellular studies, *Anal. Chem.*, **53**, 2267.
50. Chao, P., Ammann, D., Oesch, U., Simon, W. and Lang, F. (1988). Extracellular and intracellular hydrogen ion-selective microelectrode based on neutral carriers, *Pflügers Arch.*, **411**, 216.
51. Tsien, R. Y. and Rink, T. J. (1981). Ca^{2+}-selective electrodes: a novel PVC-gelled neutral carrier mixture compared with other currently available sensors, *J. Neurosci. Methods*, **4**, 73.
52. Buhrer, T., Peter, H. and Simon, W. (1988). Ammonium ion-selective microelectrode based on the antibiotics nonactin-monactin, *Pflügers Arch.*, **412**, 359.
53. Jensen, K., Revsbech, N. P. and Nielsen, L. P. (1993). Microscale distribution of nitrification activity in sediment determined with a shielded microsensor for nitrate, *Appl. Environ. Microbiol.*, **59**, 3287.
54. Koryta, J. and Stulik, K. (1983). *Ion-selective Electrodes*, 2nd edn, Cambridge University Press, Cambridge.
55. Verschuren, P. G., van der Baan, J. L., de Beer, D. and van den Heuvel, J. C. (1998). A nitrate-selective microelectrode based on a lipophilic derivative of iodocobalt (III) (salen), *Fres. J. Anal. Chem.*, **363**, 595–598.

56. Rudkevich, D. M., Stauthamer, W. P. R. V., Verboom, W., Engbersen, J. F. J., Harkema, S. and Reinhoudt, D. N. (1992). UO_2–salenes: neutral receptors for anions with a high selectivity for dihydrogen phosphate, *J. Am. Chem. Soc.*, **114**, 9671.
57. Revsbech, N. P. (1994). Analysis of microbial mats by use of electrochemical microsensors: recent advances. In *Microbial Mats*, ed. Stal, L. and Caumette, P., Springer, Berlin, Vol. **35**, p. 135.
58. Damgaard, L. R., Larsen, L. H. and Revsbech, N. P. (1995). Microscale biosensors for environmental monitoring, *Trends Anal. Chem.*, **14**, 300.
59. Sweerts, J.-P. R. A. and de Beer, D. (1989). Microelectrode measurements of nitrate gradients in the littoral and profundal sediments of a meso-eutrophic lake (Lake Vechten, The Netherlands), *Appl. Environ. Microbiol.*, **55**, 754.
60. Ross, J. W. (1969). Anion selective microelectrode. In *United States Patent Office*, Orion Research Incorporated, Cambridge, MA, USA, p. 6.
61. Meyer, T., Wensel, T. and Stryer, L. (1990). Kinetics of calcium channel opening by inositol 1,4,5-triphosphate, *Biochemistry*, **29**, 32.
62. De Beer, D., van den Heuvel, J. C. and Ottengraf, S. P. P. (1993). Microelectrode measurements of the activity distribution in nitrifying bacterial aggregates, *Appl. Environ. Microbiol.*, **59**, 573.
63. Schramm, A., de Beer, D., Wagner, M. and Amann, R. (1998). *Nitrosospira* and *Nitrospira* sp. as dominant populations in a nitrifying fluidized bed reactor: identification and activity in situ. *Appl. Environ. Microbiol.*, **64**, 3480.
64. Zhang, T. C., Fu, Y. C. and Bishop, P. L. (1994). Competition in biofilms. *Wat. Environ. Res.*, **67**, 992.
65. Santegoeds, C. M., Muyzer, G. and de Beer, D. (1998). Biofilm dynamics studied with microsensors and molecular techniques, *Wat. Sci. Technol.*, **3**, 125.
66. Schramm, A. (1998). In situ structure and function analysis of nitrifying/denitrifying biofilms, Bremen University.
67. de Beer, D., Schramm, A., Santegoeds, C. M. and Nielsen, H. K. (1998). Anaerobic processes in activated sludge, *Wat. Sci. Technol.*, **37**, 605.
68. Sweerts, J.-P. R. A., de Beer, D., Nielsen, L. P., Verdouw, H., van den Heuvel, J. C., Cohen, Y. and Cappenberg, T. E. (1990). Denitrification by sulphur oxidizing *Beggiatoa* spp. mats on freshwater sediments, *Nature*, **344**, 762.
69. Sweerts, J.-P. R. A., Bar-Gillisen, M. J., Cornelise, A. A. and Cappenberg, T. E. (1991). Oxygen consuming processes at the profundal and littoral sediment-water interface of a small meso-eutrophic lake (Lake Vechten, the Netherlands), *Limnol. Oceanogr.*, **36**, 1124.
70. Jensen, K., Sloth, N. P., Risgaard-Petersen, N., Rysgaard, S. and Revsbech, N. P. (1994). Estimation of nitrification and denitrification from microprofiles of oxygen and nitrate in model sediment systems, *Appl. Environ. Microbiol.*, **60**, 2064.
71. De Beer, D. (1998). Use of microelectrodes to measure in situ microbial activities in biofilms, sediments and microbial mats. In *Molecular Microbial Ecology Manual*, ed. Akkermans, A. D. L., van Elsas, J. D. and de Bruyn, F. J., Kluwer, Dordrecht, Vol. **8.1.3**, in press.
72. Risgaard-Petersen, N. and Jensen, K. (1997). Nitrification and denitrification in the rhizosphere of the aquatic macrophyte *Lobelia dortmanna* L., *Limnol. Oceanogr.*, **42**, 529.
73. Hartley, A. M., House, W. A., Leadbeater, B. S. C. and Callow, M. E. (1996). The use of microelectrodes to study the precipitation of calcite upon algal biofilms, *J. Colloid Interface Sci.*, **183**, 498.

74. McConnaughey, T., D. and Falk, R. H. (1991). Calcium proton exchange during algal calcification, *Biol. Bull.*, **180**, 185.
75. McConnaughey, T. D. (1991). Calcification in *Chara corallina*: CO_2 hydroxylation generates protons for bicarbonate assimilation, *Limnol. Oceanogr.*, **36**, 619.
76. Revsbech, N. P., Madsen, B. and Jørgensen, B. B. (1986). Oxygen production and consumption in sediments determined at high spatial resolution by computer simulation of oxygen microelectrode data, *Limnol. Oceanogr.*, **31**, 293.
77. Revsbech, N. P., Jørgensen, B. B. and Brix, O. (1981). Primary production of microalgae in sediments measured by oxygen microprofile, $H^{14}CO_3^-$ fixation, and oxygen exchange methods, *Limnol.Oceanogr.*, **26**, 717.
78. de Beer, D., Kühl, M., Stambler, N., and Vaki, L. (2000). A microsensor study of light enhanced CA^{2+} uptake and photosynthesis in the reef-building hermatynic coral *Favin sp. Mul. Ecol. Ploy. Series* **194**, 75
79 Köhler-Rink, S., and Kühl, M., (2000). Microsensor studies of photosynthesis and respiration in larger symbiotic foraminifera. I The physico-chemical microenvironment of *Marginopora vertebralis, Amphistegnia lobifera and Amphisoris hemprechii. Marine Biol.* In press.
80. Mathison, S. and Bakker, E. (1998). Effect of transmembrane electrolyte diffusion on the detection limit of carrier based potentiometric ion sensors, *Anal. Chem.*, **70**, 303.
81. Sokaliski, T., Ceresa, A., Zwickl, T. and Pretsch, E. (1997). Large improvement of the lower detection limit of ion-selective polymer membrane electrodes, *J. Am. Chem. Soc.*, **119**, 11347.